

Article

Assessment of Production Performance and Uncertainty in the UBGH2-6 Gas Hydrate Reservoir, Ulleung Basin

Youngmin Kim and Wonsuk Lee * 

Marine Geology and Energy Division, Korea Institute of Geoscience and Mineral Resources, Daejeon 34132, Republic of Korea; kimym@kigam.re.kr

* Correspondence: wslee@kigam.re.kr

Abstract: This study delineates the intricate dynamics of gas hydrate production in the UBGH2-6 reservoir, located in the Ulleung Basin, by deploying a comprehensive simulation model. By integrating a sensitivity analysis with Latin hypercube sampling-based Monte Carlo simulations, we evaluated the influences on gas and water production and explored the underlying uncertainties within this gas hydrate reservoir. The simulation model revealed significant findings, including the production of approximately 440 t of gas and 34,240 t of water, facilitated by a depressurization strategy at 9 MPa for a year. This highlights the pivotal roles of porosity, permeability, and thermal properties in enhancing production rates and influencing hydrate dissociation processes. Sensitivity analysis of 19 parameters provides insights into their impact on production, identifying the key drivers of increased production rates. Furthermore, uncertainty analysis examined 300 reservoir models, utilizing statistical percentiles to quantify uncertainties, projecting a median gas production of approximately 455 t. This study identifies critical factors affecting gas hydrate production and offers valuable insights for future exploration and exploitation strategies, making a significant contribution to the field of gas hydrate research.

Keywords: gas hydrate; Ulleung basin; sensitivity analysis; uncertainty analysis; Latin hypercube sampling-based Monte Carlo simulation



Citation: Kim, Y.; Lee, W. Assessment of Production Performance and Uncertainty in the UBGH2-6 Gas Hydrate Reservoir, Ulleung Basin. *J. Mar. Sci. Eng.* **2024**, *12*, 748. <https://doi.org/10.3390/jmse12050748>

Academic Editor: Hailong Lu

Received: 28 March 2024

Revised: 23 April 2024

Accepted: 26 April 2024

Published: 29 April 2024



Copyright: © 2024 by the authors. Licensee MDPI, Basel, Switzerland. This article is an open access article distributed under the terms and conditions of the Creative Commons Attribution (CC BY) license (<https://creativecommons.org/licenses/by/4.0/>).

1. Introduction

Gas hydrates are an unconventional gas resource with the potential to supply natural gas on a large scale, addressing the growing global energy demand [1–4]. Gas hydrates are crystalline solid compounds consisting of water and gas molecules. The water molecules form a cage-like structure through hydrogen bonds, encapsulating guest gas molecules stabilized by van der Waals forces [5]. Naturally occurring hydrates predominantly contain hydrocarbon molecules such as methane (CH₄), ethane (C₂H₆), and propane (C₃H₈), in addition to other gases like H₂S, N₂, and CO₂. These hydrates exist as non-flowing, crystalline solids resembling ice and are capable of efficiently storing substantial volumes of gas. One volume of methane hydrate can contain 160–180 volumes of methane gas under standard temperature and pressure conditions [6].

Hydrate dissociation methods can be classified into four main categories, based on their pressure–temperature equilibrium characteristics. The first method is depressurization, which entails reducing the reservoir pressure below the equilibrium threshold for hydrates. The second method, thermal stimulation, involves elevating the temperature beyond the hydrate equilibrium temperature. The third method incorporates the injection of chemical inhibitors, such as salts or alcohols, which modify the hydrate pressure–temperature equilibrium curve. The fourth method involves injecting gases, such as CO₂ or N₂, to facilitate the replacement of CH₄ within the hydrates. This gas replacement method serves as a strategy for CO₂ sequestration in hydrate form, thereby supporting efforts toward carbon neutrality [7].

The presence of gas hydrates in marine sediments and permafrost regions makes them a significant potential candidate in the future energy mix, possibly easing the energy crisis and aiding the transition to sustainable energy sources. Key research locations for marine gas hydrates include the South China Sea, Japan's Nankai Trough, the Ulleung Basin in the East Sea, the Pacific Ocean near Oregon, the Gulf of Mexico, and the Gulf of Oman in the Indian Ocean [8–11]. The Ulleung Basin, situated off the coast of Korea in the East Sea, has emerged as a site of considerable interest for gas hydrate exploration. Preliminary studies indicate the presence of significant gas hydrate deposits, positioning the basin as a potential hotspot for gas hydrate extraction [12,13]. In 2010, extensive deep drilling operations were conducted at 13 sites in the Ulleung Basin, employing logging-while-drilling (LWD) and measurement-while-drilling techniques and core samples were collected from these locations. The integration of geological models, seismic analyses, well logging, and core data from these deep drilling sites led to the designation of the UBGH2-6 site in the East Sea, for trial production [12].

The Korea Institute of Geoscience and Mineral Resources (KIGAM) and several other institutions have been actively engaged in pioneering research on the pilot production of gas hydrates within the UBGH2-6 area. In this region, gas hydrate production via depressurization is under investigation, owing to its technical reliability and efficiency in accelerating hydrate dissociation reactions. Various studies on depressurization methods have been conducted, targeting UBGH2-6 [14–17]. Moridis et al. [14] employed the TOUGH + HYDRATE simulator, developed by the Lawrence Berkeley National Laboratory (LBNL), to analyze gas hydrate production trends and simulate formation subsidence linked to depressurization. Moridis et al. [15] investigated the feasibility of gas hydrate production by considering the properties and conditions of UBGH2-6. They examined the sensitivity of the system to heterogeneity in permeability, porosity, and initial hydrate saturation and assessed the geomechanical response to a 14-d production period. Studies have revealed that production efficiency is significantly influenced by various depressurization conditions, such as bottomhole pressure (BHP) and the rate of depressurization [16]. Furthermore, studies have shown that, in sediments with a hydrate saturation exceeding 70%, pressure propagation becomes erratic, leading to a slow dissociation rate. Lee et al. [17] explored the effects of bottomhole pressure and production duration under cyclic depressurization and found that cyclic depressurization at 6 MPa, compared to continuous depressurization at 9 MPa, maintains a similar formation vertical displacement and tripled the cumulative gas output. However, these investigations were primarily focused on the controllable aspects of the depressurization method, potentially overlooking other influencing factors.

Gas hydrate reservoirs are embedded within complex geological formations, resulting in a significantly heterogeneous gas hydrate distribution. The feasibility of gas hydrate production depends on the ability to sustainably extract gas. Conducting uncertainty analyses is crucial for generating precise assessments of productivity, considering the variability in production rates and the influence of geological uncertainties on the efficiency of gas hydrate extraction processes. Monte Carlo simulations are used for analyzing the impact of uncertainties in reservoir properties on gas hydrate production [18,19]. Nakajima et al. [18] explored the effects of 22 reservoir parameters on the cumulative gas production at the Kuparuk 7-11-12 site, within the Prudhoe Bay Unit on the Alaska North Slope, identifying relative gas permeability and residual gas saturation as notably sensitive parameters. Gaddipati [19] conducted an uncertainty evaluation focusing on reservoir parameters at the Walker Ridge 313 deposit in the Gulf of Mexico, using Latin hypercube Monte Carlo sampling. The results of these studies highlight the crucial role of uncertainty assessments in revealing the production potential of gas hydrates, through a detailed examination of reservoir parameters.

UBGH2-6 is a Class 3 type gas hydrate reservoir consisting of 14 hydrate-bearing sands (HBSs). The HBS layers are notably thin and delineated by layers of low-permeability mud. The hydrate saturation levels across the HBSs vary significantly from 38.8% to 86.2%, demonstrating pronounced vertical heterogeneity. Additionally, the forecasting of gas

and water production in UBGH2-6 is challenging because of the inherent uncertainty in reservoir parameters. Despite the need for uncertainty analysis to guide the design of pilot production, such studies are lacking.

This study developed a reservoir simulation model to analyze hydrate dissociation and gas production characteristics in the UBGH2-6 gas hydrate reservoir. Sensitivity analysis factors were selected based on the reservoir and fluid properties for the construction of the base model and the analysis determined the impact of each factor on hydrate production. Moreover, by identifying variables with high sensitivity and employing efficient Monte Carlo simulations for uncertainty analysis, essential information for evaluating production efficiency was obtained and risks were managed in UBGH2-6.

2. Methods

2.1. Methodology

Figure 1 shows the methodology used for the sensitivity and uncertainty analyses of the gas hydrate reservoirs at the UBGH2-6 site. To conduct this analysis, reservoir simulations were performed to explore the dissociation of gas hydrates and the resulting fluid production volumes. This process used integrated geological modeling, seismic interpretation, drilling data, well log data, and core sample analyses from the UBGH2-6 site, to construct an accurate reservoir model.

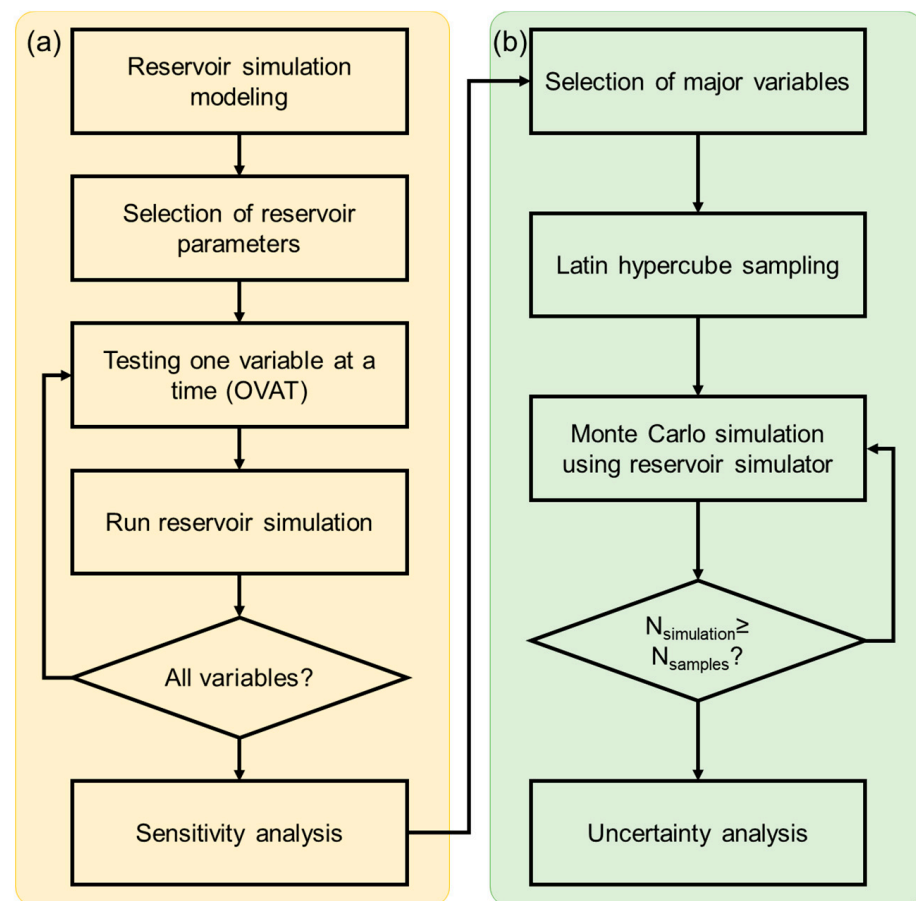


Figure 1. Methodology for sensitivity and uncertainty analysis in gas hydrate reservoirs. (a) Performing sensitivity analysis on all selected reservoir parameters using the one-variable-at-a-time (OVAT) approach; (b) selecting major variables with high sensitivity and analyzing reservoir property uncertainty through Latin hypercube sampling-based Monte Carlo simulation.

Reservoir modeling involves various parameters, including rock physics, rock–fluid interactions, and initial conditions, such as pressure and temperature. Because of the

challenges in obtaining these properties from laboratory experiments and field data, some variables are estimated or arbitrarily set, introducing inherent uncertainties. This study identifies properties with significant uncertainties and evaluates their impact on the productivity of gas hydrate reservoirs via sensitivity analysis. To this end, we employed the one-variable-at-a-time (OVAT) method. Reservoir simulations were conducted for each variable and a tornado chart was used to assess the impact of each variable on the cumulative gas production.

Variables that showed significant sensitivity to cumulative gas production were identified as key variables. Considering the limited field test data available for UBGH2-6, these key variables were assumed to follow uniform distributions. The traditional approach to Monte Carlo simulations requires numerous samples and can, therefore, be resource-intensive. Latin hypercube sampling (LHS) significantly enhances the efficiency of Monte Carlo simulations, by reducing the number of samples required. In this study, LHS was employed to select 300 cases to execute Monte Carlo simulations, using the TOUGH+HYDRATE simulator. The use of histograms and probability distributions enabled an in-depth examination of gas and water production volumes, particularly through the calculation of P10, P50, and P90. This methodology effectively quantified the uncertainties present in the gas hydrate reservoirs of UBGH2-6.

2.2. Reservoir Simulation for UBGH2-6

In this study, the UBGH2-6 gas hydrate reservoir was modeled using the TOUGH + HYDRATE simulator, which is well known for its comprehensive capability to simulate fluid and heat flow dynamics, the phase behavior of fluids, thermodynamic transformations, and reactions associated with hydrate formation and dissociation in gas hydrate reservoirs. The TOUGH + HYDRATE simulator developed by Lawrence Berkeley National Laboratory is a fully implicit compositional model, adept at handling the nonlinear complexities associated with natural gas hydrate processes. Its capacity to manage heat and mass transfer across gas, aqueous liquid, ice, and hydrate phases, as well as to simulate all 15 thermodynamic states of the $\text{CH}_4 + \text{H}_2\text{O}$ system, makes it highly effective for various hydrate dissociation methods such as depressurization, thermal stimulation, and inhibitors [5,20]. This versatility is crucial in accurately predicting hydrate behavior under diverse environmental conditions and in complex geological settings. The robustness of T + H in modeling strong nonlinearities and handling phase transitions and sharp solution gradients ensures its utility in both experimental setups and real-world gas hydrate exploitation, validated by extensive testing and documentation in the scientific literature [5,20–25].

Figures 2 and 3 show schematics of the UBGH2-6 gas hydrate reservoir model, developed from a detailed stratigraphic framework. The model delineates HBSs located between depths of -140.5 m and -153.8 m, relative to the sea floor (water depth 2157 m). As illustrated in Figure 3, the HBS, of 13.3 m thick, comprises interbedded sand and mud layers, with hydrates occurring exclusively within the sand strata. These sand strata consist of 14 distinct layers, each varying in thickness from 0.1 m to 0.6 m, indicating notably thin beds. These layers were sequentially designated from gas hydrate-bearing sand (GHS) layer 1, the uppermost layer, to layer 14, the lowest layer.

The initial hydrate saturation within the UBGH2-6 reservoir exhibited significant variability across its sandy layers, with percentages ranging from 38.8% to 86.2%. This variability is crucial for understanding the dynamics of hydrate dissociation and gas production within the reservoir. Previous studies [26,27] have investigated the influence of initial hydrate saturation on both the advancement of the dissociation front and subsequent gas production, focusing on one-dimensional core models and sub-sea hydrate reservoir models off the coast of Uruguay. These studies concluded that, at high hydrate saturation levels, specifically within the 70–80% range, the effective permeability is significantly reduced. This reduction in permeability leads to a negligible amount of gas production through depressurization techniques, thereby identifying a critical saturation threshold for gas hydrates within the aforementioned range.

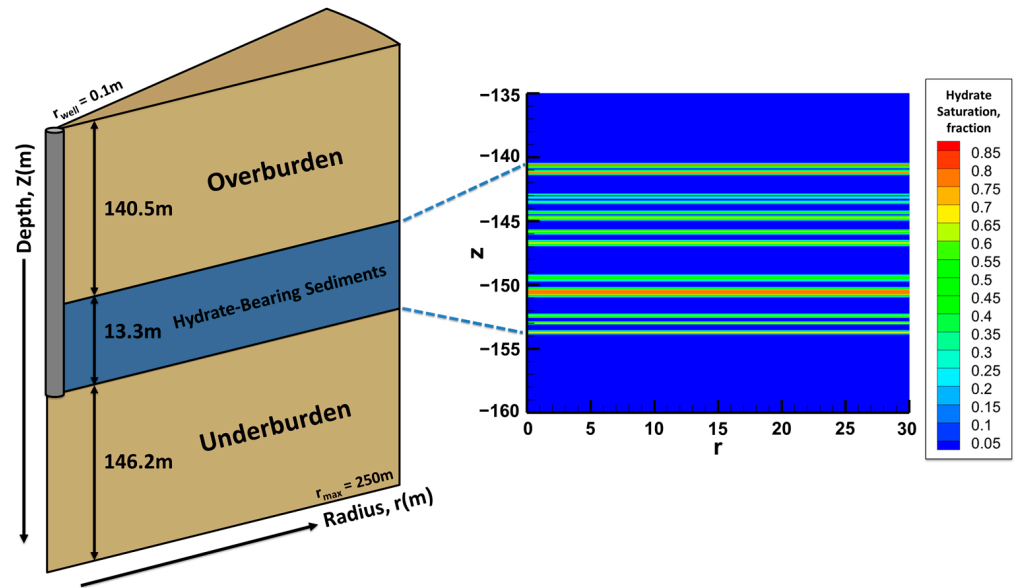


Figure 2. Schematic diagram of the cylindrical system(left) and initial gas hydrate saturation distribution (right) in the UBGH2-6 reservoir.

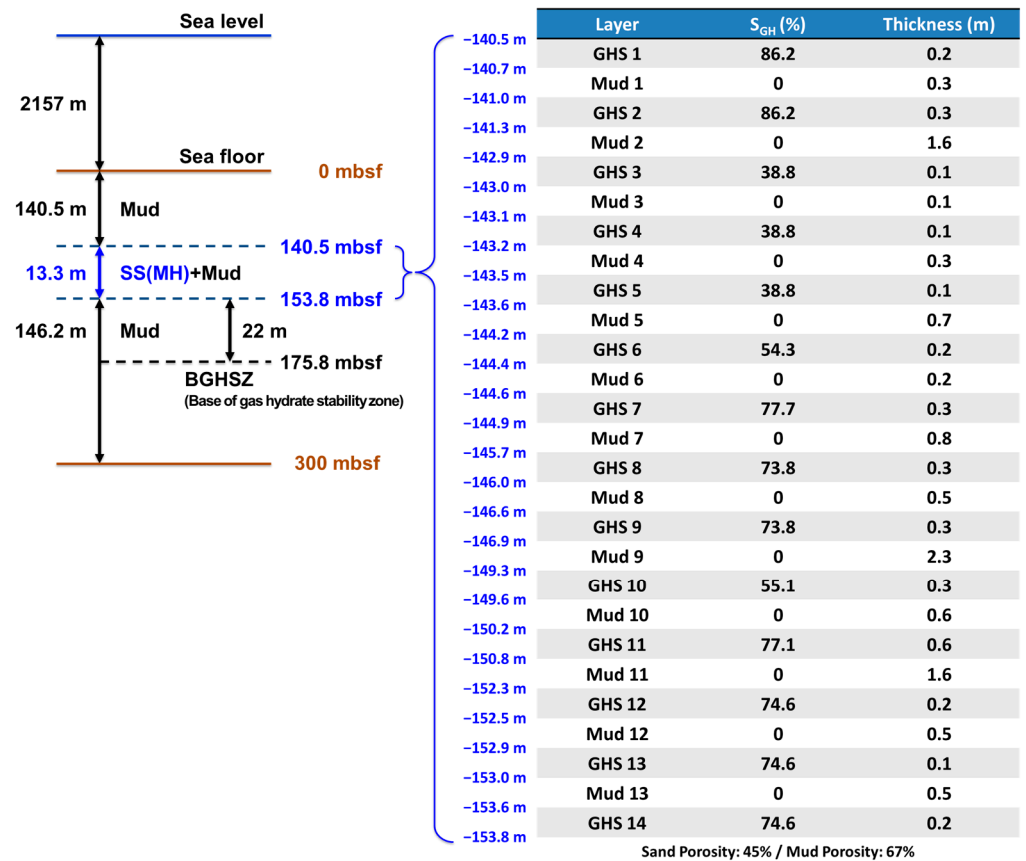


Figure 3. Geological stratification of the UBGH2-6 deposit. (Left) The UBGH2-6 area, located at a water depth of 2157 m, features a gas hydrate reservoir positioned 140.5 m below the sea floor. The reservoir lies above the base of the gas hydrate stability zone (BGHSZ), ensuring the stable presence of hydrates. (Right) The reservoir, with a thickness of 13.3 m, comprises 14 sand layers interspersed with 13 mud layers. The hydrate saturation within the sand layers varies from 38.2% to 86.2%.

In the context of the UBGH2-6 reservoir, an important observation is that 9 out of the 14 sand layers have initial hydrate saturations exceeding 70%. This underscores the importance of conducting detailed analyses of the propagation of the hydrate dissociation front and the associated gas production across each distinct sand layer. Such analyses are pivotal for identifying the critical hydrate saturation level specific to the UBGH2-6 environment and for elucidating the contributory role of each sand layer in the overall gas production within the reservoir. Understanding these dynamics is instrumental for optimizing production strategies and enhancing the efficiency of gas extraction from hydrate-bearing sediments.

To accurately simulate hydrate dissociation and gas flow, the reservoir model for UBGH2-6 employs a cylindrical grid configuration. This includes 150 grids radially (r-direction) and 96 grids in depth (z-direction), for a total of 14,400 grids. Radially, the cylindrical grid extends to 250 m, with the grid length gradually increasing from an initial 0.05 m at the center, to accommodate the geometric complexities of the model. The boundary conditions included a no-flow boundary at a radial distance of 250 m and a constant temperature boundary at depths of 0 and 300 m, ensuring a realistic simulation environment for investigating the hydrate behavior within the UBGH2-6 reservoir.

The reservoir characteristics of UBGH2-6 are presented in Table 1. Porosity measurements, derived from LWD and core analyses, indicated a porosity of 45% for sand layers and 67% for mud layers. Permeability contrasts are also stark, with sand layers exhibiting a permeability of 180 md, significantly higher than the 0.2 md measured in the mud layers. The adopted base model incorporates the van Genuchten approach to model relative permeability and capillary pressures. Permeability anisotropy is the difference between the horizontal and vertical permeabilities within a reservoir. In cases where the horizontal and vertical permeabilities were assumed to be equivalent, the base model designated the value of this parameter as 1.

Table 1. Reservoir and fluid properties of the UBGH2-6 base model.

Parameters		Value
Overburden thickness, m		140.5
Underburden thickness, m		146.2
HBS thickness, m		13.3
Porosity, fraction	Sand	0.45
	Mud	0.67
Permeability, md	Sand	180
	Mud	0.2
Permeability anisotropy ratio		1
Permeability reduction factor		6
Specific heat		830
Thermal conductivity (sand), W/m/k		1.45
Thermal conductivity (mud), W/m/k		1
Hydrate saturation (sand layer), fraction		0.388~0.862
Relative permeability model (van Genuchten)	$k_{rA} = \sqrt{S^*} \left\{ 1 - \left(1 - [S^*]^{1/\lambda} \right)^\lambda \right\}^2$	
	$k_{rG} = \sqrt{1 - S^*} \left\{ \left(1 - [S^*]^{1/\lambda} \right)^\lambda \right\}^2$	
	$S^* = \frac{S_A - S_{irA}}{S_{mxA} - S_{irA}}$	

Table 1. Cont.

Parameters		Value
Irreducible water saturation (S_{irA})	Sand	0.1
	Mud	0.1
Irreducible gas saturation (S_{irG})	Sand	0.01
	Mud	0.01
Exponent (λ)	Sand	0.66
	Mud	0.75
Capillary pressure model (van Genuchten)		$P_{cap} = -P_0 \left[(S^*)^{-1/\lambda} - 1 \right]^{-\lambda}$ $S^* = \frac{S_A - S_{irA}}{S_{mA} - S_{irA}}$
Exponent (λ)	Sand	0.66
	Mud	0.75
P_0 , MPa	Sand	0.01
	Mud	0.02
Well radius, m		0.1
Bottomhole pressure, MPa		9
Depressurization rate, MPa/h		0.5

A key aspect of the modeling effort involved the application of the Masuda et al. [28] model, to describe the impact of hydrate saturation on absolute permeability. This relationship is quantified using Equation (1), which delineates the reduction in permeability as a function of hydrate saturation (S_H). The permeability reduction index (N) is set within a range of 3 to 25 [29]. This range varies depending on the occurrence position of hydrate within the pore space, such as grain coating and pore filling, with values above 5 being applicable for pore-filling hydrates [29,30]. For the UBGH2-6 base model, which demonstrates pore-filling features, the permeability reduction index is set at 6.

$$k_r = (1 - S_H)^N \tag{1}$$

The gas composition of the reservoir is exclusively methane, with water salinity determined to be 3.45 wt%, reflecting the geochemical conditions. The hydration number for methane hydrates was set at 6, within the established range of 5.75 to 6.2, for the base case model. Additionally, the effect of 3.45 wt% saline water was considered, acting as a chemical inhibitor that can alter the hydrate equilibrium curve. Furthermore, the equilibrium mode was chosen for hydrate dissociation, to accommodate the requirements of field-scale simulations. The initial reservoir pressure, estimated using the hydrostatic method, is 23.6 MPa, while the initial reservoir temperature, determined from a temperature gradient of approximately 112 °C/km, is calculated to be 34.08 °C. These conditions firmly place the reservoir within the hydrate stability zone, underscoring its thermodynamic favorability for hydrate existence. The initial conditions assumed that the sand layers were fully saturated with hydrate and water and, upon the application of depressurization, hydrate dissociation occurred, leading to gas–water flow.

Reflecting on the hydrate distribution within UBGH2-6, this reservoir exemplifies a Class 3 type sedimentary configuration, characterized by hydrate-bearing layers ensconced between strata of low permeability, such as shale [31,32]. Depressurization, which is unique for its operational stability and the rapid initiation of hydrate dissociation due to effective pressure dissemination, stands out as the premier production strategy for Class 3 gas hydrate reservoirs [14,22].

In line with these considerations, depressurization was selected as the principal production technique in this study. Kim et al. [33] investigated the stability of UBGH2-6 under BHP values of 5, 9, and 14 MPa, using a self-developed simulation. The criterion for good stability hinged on ensuring the compressive stress exerted on the 9 5/8" casing did not surpass its yield stress. Findings from a 14-d production trial underscored that maintaining a BHP of 9 MPa effectively maintained the compressive stress within safe limits, thereby confirming the integrity of the well for gas extraction. Conversely, a reduction in BHP to 5 MPa significantly increased compressive stress, amplifying the potential for casing impairment. Based on the insights provided by Kim et al. [33], a threshold BHP of 9 MPa was established for the depressurization process in this reservoir. The depressurization rate, transitioning from the initial reservoir pressure to the targeted BHP, was implemented at 0.5 MPa per hour, aligning with the operational parameters conducive to maintaining good stability and optimizing gas production efficacy.

2.3. Selection of Reservoir Parameters

In this study, 11 geological and petrophysical properties were identified for sensitivity analysis, as presented in Table 2. The analysis categorized the HBS into two primary geological units—sand and mud layers. Except for the permeability anisotropy ratio, permeability reduction factor, and specific heat, the remaining eight properties were evaluated across geological units. Table 2 presents a comprehensive set of 19 parameters, corresponding to the 11 properties targeted in the sensitivity analysis.

Table 2. Selection of geological and petrophysical properties for sensitivity analysis.

Parameters		Range		
		Min	Base	Max
Porosity, fraction	Sand	0.36	0.45	0.54
	Mud	0.536	0.67	0.804
Permeability, md	Sand	144	180	216
	Mud	0.16	0.2	0.24
Permeability anisotropy ratio		0.6	0.8	1 ¹
Permeability reduction factor		4.8	6	7.2
Specific heat		664	830	996
Thermal conductivity, W/m/k	Sand	1.16	1.45	1.74
	Mud	0.8	1	1.2
Irreducible water saturation (S_{irA})	Sand	0.08	0.1	0.12
	Mud	0.08	0.1	0.12
Irreducible gas saturation (S_{irG})	Sand	0.008	0.01	0.012
	Mud	0.008	0.01	0.012
Relative permeability (RP) exponent (λ)	Sand	0.528	0.66	0.792
	Mud	0.6	0.75	0.9
Capillary pressure (CP) exponent (λ)	Sand	0.528	0.66	0.792
	Mud	0.6	0.75	0.9
P_0 , MPa	Sand	0.008	0.01	0.012
	Mud	0.016	0.02	0.024

¹ In the base model, the permeability anisotropy ratio was assigned its maximum value of 1. Sensitivity analyses were subsequently conducted for the ratios of 0.6 and 0.8, to evaluate their impact.

These parameters were selected based on either a lack of laboratory and field test data or the presence of uncertainties highlighted in previous studies. Due to insufficient data

to justify a normal or triangular distribution, a uniform distribution was assumed for all parameters. The minimum and maximum values for these distributions were set at $\pm 20\%$ relative to the base values, providing a systematic approach to assess the impact of each parameter within the scope of the sensitivity analysis.

2.4. OVAT

The OVAT method is widely used in experimental design and data analysis across various disciplines, including oil and gas research. It aims to simplify the understanding of the effect of specific variables on outcomes and assess the interactions between variables in complex systems by altering one variable at a time, while maintaining all others constant. This approach enables an independent assessment of the impact of each variable on the results.

The advantage of the OVAT method lies in its simplicity and intuitiveness, enabling an understanding of the individual impact of variables within complex systems. However, a limitation of this approach is its inability to consider the interactions between variables. In this study, the OVAT approach was employed to analyze the individual impacts of 19 reservoir parameters on gas and water production. Through the illustration of tornado charts for cumulative production, we identified variables with high sensitivity, among 19 reservoir parameters.

2.5. Latin Hypercube Sampling-Based Monte Carlo Simulation

LHS is an advanced statistical technique designed to generate quasirandom samples of parameter values from multidimensional distributions [34]. LHS significantly enhances the efficiency of Monte Carlo simulations by reducing the number of samples required. This method uses uniformly distributed samples across each parameter to ensure a thorough and equitable exploration of the input space. The ability to draw samples from any preferred probability distribution, including uniform or normal, renders LHS versatile for analyzing a wide range of data and systems.

Unlike random sampling, LHS reduces result variability, while maintaining sample correlation, thus improving the reliability of analyses and enabling more accurate uncertainty estimations. LHS is particularly beneficial for conducting uncertainty analysis within multivariable systems, because it enables the simultaneous consideration of numerous parameters. This feature renders LHS unique for evaluating uncertainties in complex systems, providing a method for understanding and mitigating potential risks. Therefore, LHS was chosen as the sampling strategy in this study, leveraging its advantages of increasing the efficiency of Monte Carlo simulations, reducing the variability in the analytical results, and facilitating the comprehensive examination of numerous parameters.

3. Results and Discussion

3.1. Reservoir Simulation Results

After a BHP of 9 MPa was maintained for a year, the resulting dissociation reactions and fluid flow dynamics within the gas hydrate reservoir were meticulously examined. Figure 4 shows the evolution of pressure, temperature, and hydrate saturation levels within the gas hydrate reservoir throughout the depressurization process. As shown in Figure 4a, initiating a 9 MPa BHP leads to the propagation of pressure from the vicinity of the wellbore. This pressure propagation, upon reducing the reservoir pressure beneath the hydrate equilibrium pressure threshold, fosters favorable conditions for hydrate dissociation. As an endothermic process, the hydrate dissociation induces a temperature reduction near the wellbore, as shown in Figure 4b.

A closer examination of individual sand layers revealed that hydrate dissociation and subsequent gas production predominantly commenced within GHS layers 3–5, which were characterized by relatively low hydrate saturations. Conversely, among GHS layers 12–14, which have the same hydrate saturation, GHS layer 13, was unique for its narrow sand layer thickness, exhibiting a predisposition toward preferential dissociation. This analysis

underscores the interaction between physical reservoir characteristics and the dynamics of hydrate dissociation and gas production under controlled depressurization conditions.

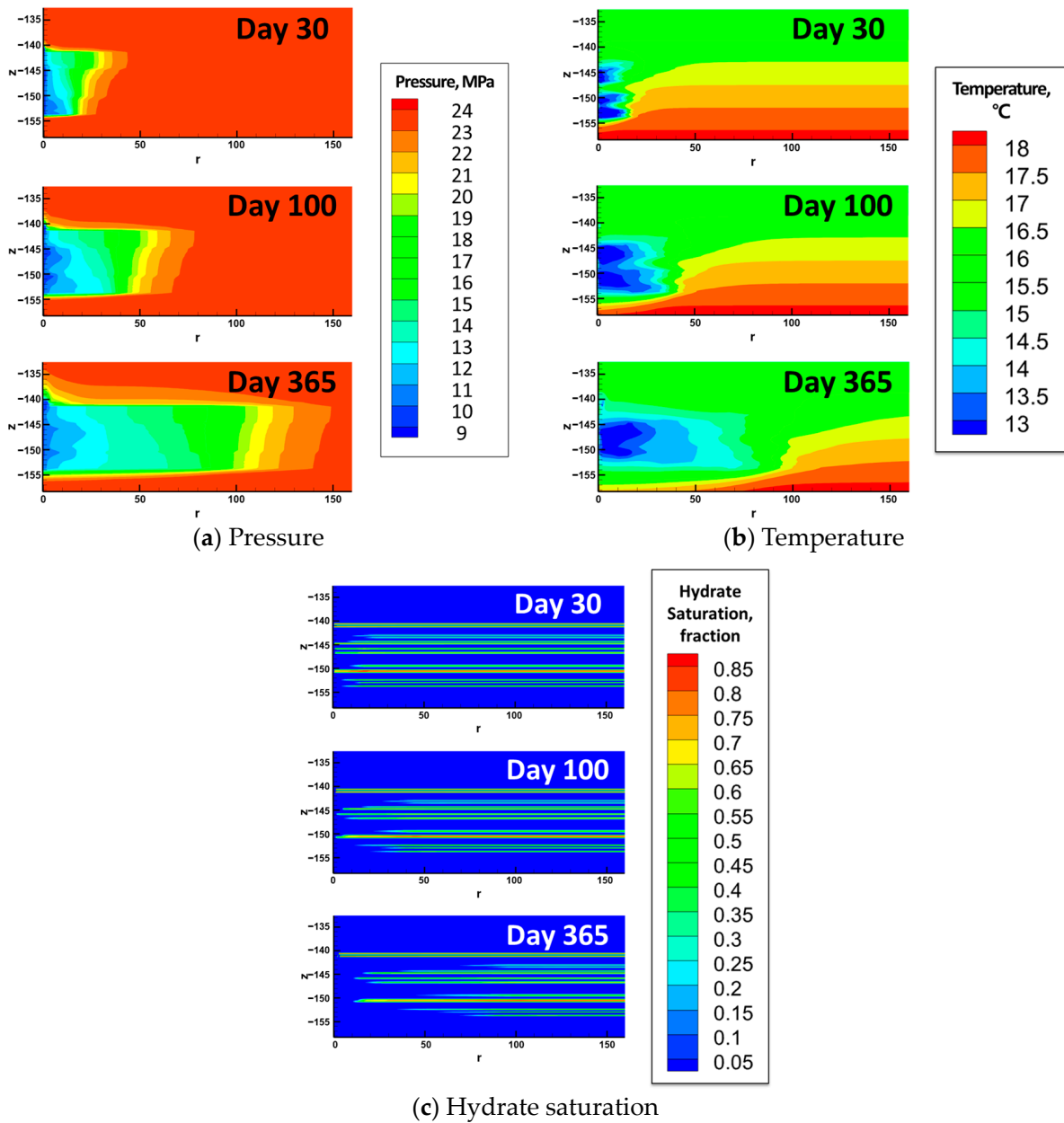


Figure 4. Radial depth plane analysis of pressure, temperature, and hydrate saturation variations throughout the 365-day production period.

The temporal evolution of gas and water production from UBGH2-6 is shown in Figure 5. Gas production exhibited a consistent increase, reaching a peak rate of 0.016 kg/s by day 250. Initially, the rate of gas production surged, but began to decelerate after the first 100 days. This deceleration is attributed to the reduced rate of pressure propagation within the initially dissociated GHS layers 3–5 and 12–14, as hydrate dissociation expanded across the entire HBS. We presumed that no free gas was present under the initial reservoir conditions, suggesting that all the produced gas originated from hydrate dissociation. Under a maintained BHP of 9 MPa in the UBGH2-6 gas hydrate reservoir, the gas production amounted to 439,932 kg.

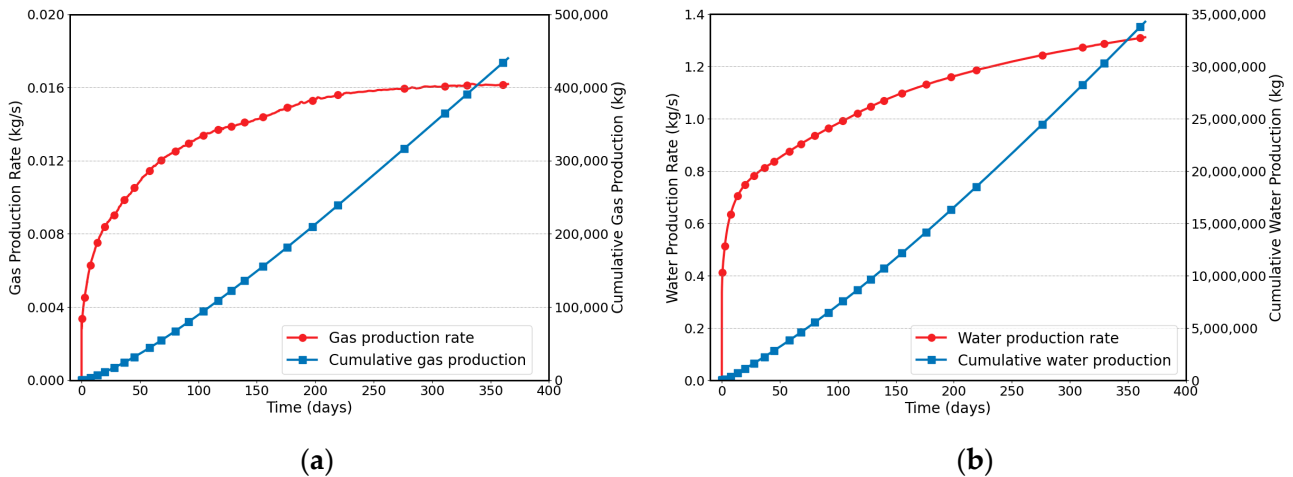


Figure 5. Gas (a) and water (b) production over time during the 365-day production test.

As shown in Figure 5b, water production exhibited a consistent upward trend, culminating at a peak rate of 1.3 kg/s after the production period. Notably, no deceleration was observed in the water production rate. Given that the reservoir initially contained water, the sustained increase in water production can be attributed to the generation of additional water, due to hydrate dissociation. As a result, the cumulative water production amounted to 34,240,600 kg, highlighting the significant contribution of hydrate dissociation to the water output in the UBGH2-6 reservoir.

The production from each layer of UBGH2-6 can be represented by its contribution to the total production obtained from a single production well. Analyzing the layer-specific production within the HBS of UBGH2-6 enables the identification of gas production characteristics in reservoirs with discontinuous hydrate distributions in sand layers and also enables the analysis of the impact of structural changes in a specific layer on adjacent sand layers. Figure 6 shows the daily gas production from each layer of the HBS. In the UBGH2-6 gas hydrate reservoir, notable production was absent in both GHS layers 1 and 2, as well as the mud layers. Although the mud layers did not contain hydrates, the gas generated from the dissociating hydrates in neighboring GHS layers migrated through them.

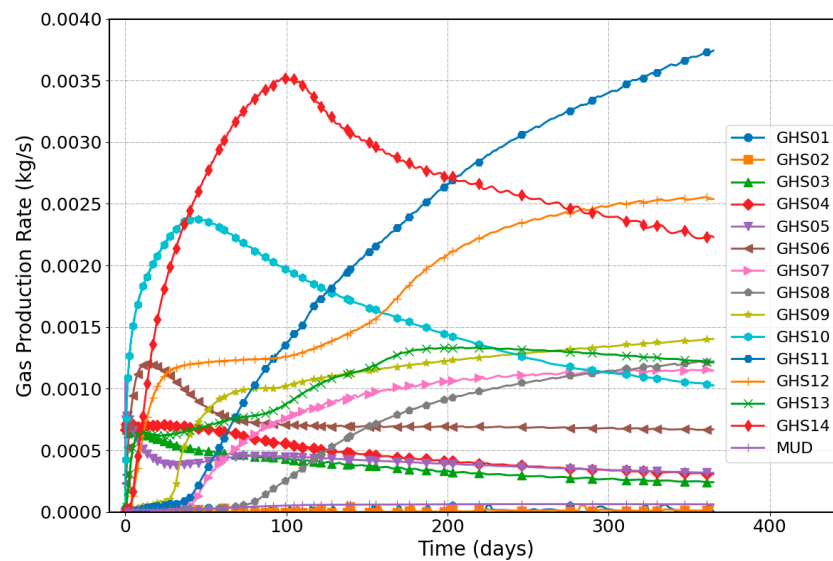


Figure 6. Gas production rate of each layer during the 365-day production test.

Gas production in GHS layers is influenced by the thickness of each layer and the initial hydrate saturation. Hydrate dissociation in GHS layers 3–5 was rapid, as shown in Figure 4c. However, the production rate remained under 0.001 kg/s, because of the low hydrate saturation of 38.8%. Gas production began immediately upon depressurization of GHS layers 6 and 10. The hydrate saturation levels of these layers were 54.3% and 55.1%, respectively, which were conducive to hydrate dissociation. In contrast, gas production in GHS layers 7–9 commenced between 30 and 70 days after production initiation. These layers, characterized by a hydrate saturation exceeding 70% and a thickness of 0.3 m, demonstrated that hydrate dissociation is not immediate and necessitates an adequate period of depressurization. Although GHS layer 11, with its thick layer and high hydrate saturation, did not produce gas immediately, its production significantly surged once dissociation began, owing to the extensive volume of hydrates.

Notably, a high level of hydrate saturation did not unilaterally slow the dissociation rates. Despite a hydrate saturation of 74.6%, GHS layers 12–14 initiated immediate gas production, which was attributed to their thin layer characteristics. GHS layer 14 underwent a shift in its production trend around day 90, but continued to demonstrate a robust gas production rate. Depressurization in a specific GHS can impact the pressure reduction in adjacent GHS layers. Consequently, in gas hydrate reservoirs such as UBGH2-6, which exhibit a stratified arrangement of multiple GHS layers, the interlayer spacing emerges as a critical factor for subsequent analysis.

As shown in Figure 4c, the depressurization process delineates two distinct zones within the GHS layers—the dissociated zone and the gas hydrate zone [26]. The boundary between these zones is defined by the hydrate dissociation front, which progressively moves away from the production well as hydrate dissociation occurs. The advance of the dissociation front serves as a direct measure of the gas recovery efficacy, since hydrates within the dissociated zone are completely transformed into water and natural gas for production [35]. Table 3 presents a detailed summary of the hydrate dissociation front propagation distance and cumulative gas production across each sand layer in the UBGH2-6 reservoir. Notably, GHS layers 3–5 exhibited the most rapid progression of the dissociation front, extending radially between 68 and 83 m by the end of the production period. An analysis of the layers undergoing hydrate dissociation revealed hydrate saturations ranging from 38.8% to 55.1%, with sand layer thicknesses between 0.1 and 0.2 m. Despite the 0.3 m thickness of GHS layer 10, its relatively low hydrate saturation of 55.1% underscores the trend that thin sand layers with low hydrate saturations facilitate efficient hydrate dissociation and gas production.

Table 3. Results of hydrate dissociation front and cumulative gas production of UBGH2-6.

Domain	Thickness, m	Hydrate Saturation, %	Maximum Dissociation Front, m	Cumulative Gas Production, kg
GHS 1	0.2	86.2	2	303
GHS 2	0.3	86.2	3	319
GHS 3	0.1	38.8	82	11,668
GHS 4	0.1	38.8	68	14,781
GHS 5	0.1	38.8	83	12,539
GHS 6	0.2	54.3	36	23,379
GHS 7	0.3	77.7	16	26,818
GHS 8	0.3	73.8	11	21,867
GHS 9	0.3	73.8	18	34,054
GHS 10	0.3	55.1	46	49,659
GHS 11	0.6	77.1	10	68,811

Table 3. Cont.

Domain	Thickness, m	Hydrate Saturation, %	Maximum Dissociation Front, m	Cumulative Gas Production, kg
GHS 12	0.2	74.6	36	57,395
GHS 13	0.1	74.6	58	34,363
GHS 14	0.2	74.6	70	82,302
Muds	10	0	0	1675
Total				439,932

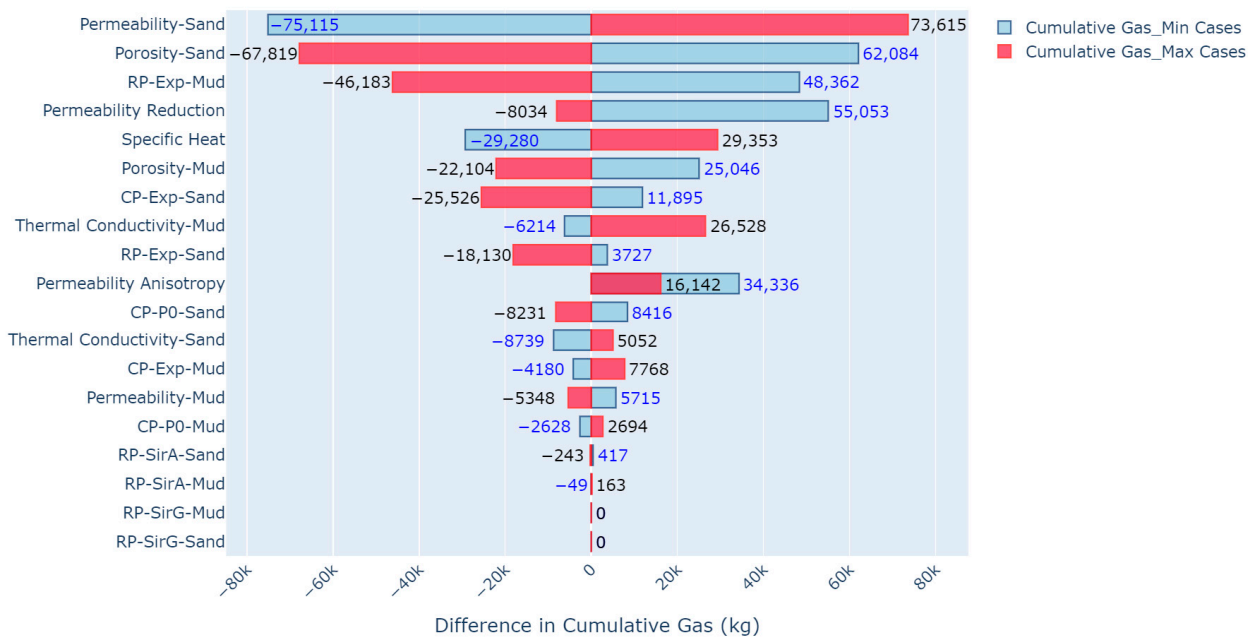
This observation aligns with the findings of Zheng et al. [26] and Tomasini and Stephen [27], who suggested that high hydrate saturations reduce the pore space availability for fluid flow, thereby diminishing effective permeability. Consequently, layers with low hydrate saturation under uniform absolute and relative permeability conditions demonstrate enhanced fluid production and pressure propagation capabilities, resulting in increased gas production. Notably, under equivalent saturation conditions, hydrate dissociation and gas production are preferentially initiated in thinner layers, because thicker hydrate-bearing layers require sufficient energy for dissociation.

3.2. Sensitivity Analysis

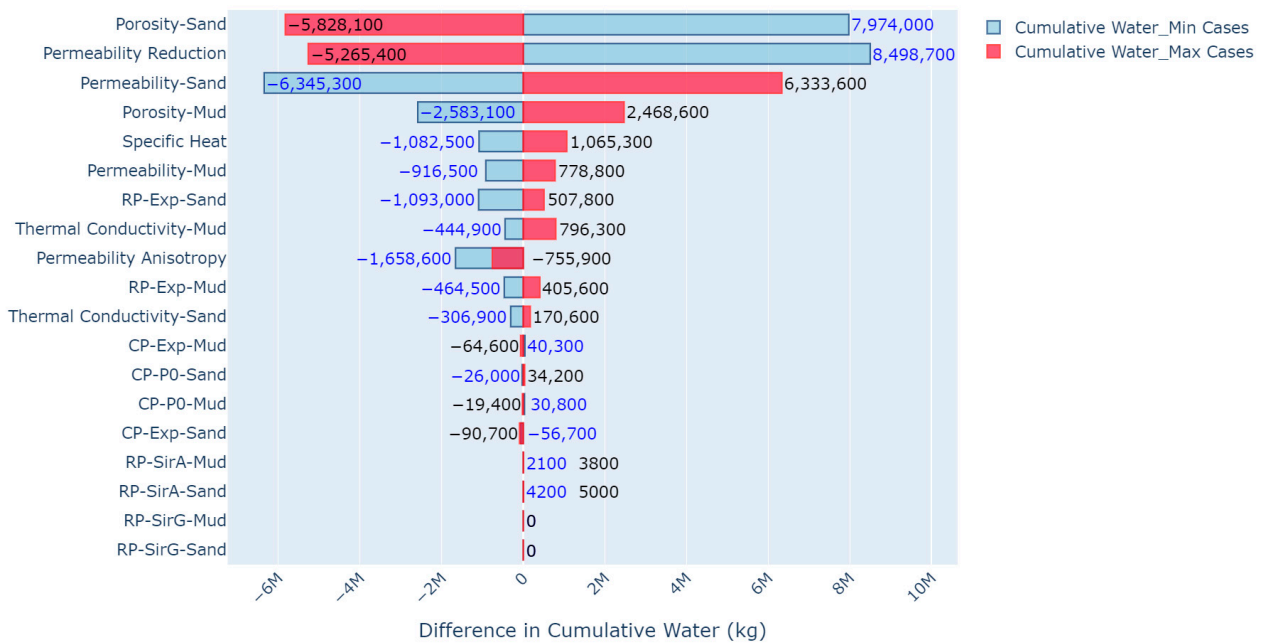
The sensitivity analysis focused on the sensitivity of the reservoir and fluid flow parameters presented in Table 2 to the cumulative gas and water production. To assess the range of impact, 38 simulations were performed, covering the minimum and maximum cases for each of the 19 parameters. Figure 7 shows the influence of these 19 parameters on the cumulative production of gas and water, utilizing tornado charts for visualization. The x-axis in Figure 7 quantifies the variation from the baseline model with a value of 0, indicating that alterations in the value of a parameter do not affect the production volumes relative to the base model. In contrast, deviations from 0 on the x-axis signify a pronounced effect of the parameter on production volumes.

Figure 7a shows the results of the sensitivity analysis focused on cumulative gas production, with parameters ranked based on the magnitude of variation observed between their minimum and maximum scenarios. Higher-ranked parameters are indicative of a stronger influence on cumulative gas production. An increase in porosity led to a corresponding increase in the volume of gas hydrates, which significantly influenced the cumulative production of both gas and water. Sand permeability has emerged as one of the most sensitive factors underlining the critical role of efficient depressurization propagation in hydrate production. The importance of permeability is highlighted by the prerequisite for the initial production of water and gas from pore spaces to enable the spread of depressurization.

Similarly, the impact of the variables affecting effective permeability, including the permeability reduction factor, relative permeability index, and permeability anisotropy, was significant. As delineated by the van Genuchten model for relative permeability, a decrease in the exponent leads to an enhanced relative permeability. Diminishing the relative permeability index for the mud layers results in an increased relative permeability in these layers, facilitating the production of gas dissociated from the sand layers through the mud layers, thereby augmenting the efficiency of gas production from the sand layers. The reduction in permeability in Equation (1) follows an exponential decay pattern, implying that an increase in the exponent yields only slight deviations from the base model. However, decreasing the exponent markedly amplified the permeability reduction effect, consequently boosting production levels.



(a)



(b)

Figure 7. Results of the sensitivity analysis for 19 parameters. (a) The cumulative gas production, and (b) the cumulative water production. The analysis results for the minimum scenario are depicted in blue, while those for the maximum scenario are indicated in red.

The endothermic reaction triggered by gas hydrate dissociation decreases the thermal energy within the formation, thereby hindering further dissociation of hydrates. Consequently, the roles of specific heat and thermal conductivity are critical. A decline in specific heat is directly associated with a decrease in cumulative gas production, thereby establishing a proportional relationship. This implies that with a low specific heat, less heat is required to induce a substantial temperature shift, adversely affecting hydrate dissociation. However, a high specific heat ensures minimal temperature fluctuations in response to the same quantity of heat absorption or release, effectively reducing the

repercussions of the endothermic reaction. Additionally, enhanced thermal conductivity indicates a more efficient heat transfer through the material. This facilitated swift thermal replenishment from the adjacent formation, even in the presence of endothermic reactions, thereby contributing positively to gas production.

Within the subgroup of variables exhibiting low sensitivity, factors related to relative permeability and capillary pressure demonstrated minimal impact. Specifically, variations of $\pm 20\%$ in irreducible gas and water saturation had negligible effects on cumulative gas production. This minimal impact is likely attributed to the low base value of irreducible gas saturation.

The analysis of the cumulative water production presented in Figure 7b demonstrates results analogous to those of the gas production scenarios, highlighting the significant influence of permeability on water production. This increased sensitivity to permeability is attributed to the higher viscosity of water than that of gas, which renders water more affected by permeability changes. Significantly, with an increase in permeability reduction, the distinction between water and gas production became more pronounced. Moreover, a decrease in the permeability anisotropy ratio, which reflects disparities between horizontal and vertical permeabilities, leads to a noticeable decrease in water production volumes.

Although the effects of the 19 parameters on the cumulative production of gas and water varied, grouping them by high and low sensitivity uncovered consistent traits. In addition to the relative permeability index, other parameters associated with relative permeability and capillary pressure (such as irreducible gas and water saturation and P_0 for the capillary pressure model) showed minimal sensitivity. This indicates that the level of uncertainty introduced by these parameters in gas hydrate production is relatively low. Thus, this study undertook an uncertainty analysis focusing on 12 variables, including porosity, permeability, permeability anisotropy ratio, permeability reduction factor, specific heat, thermal conductivity, and relative permeability index.

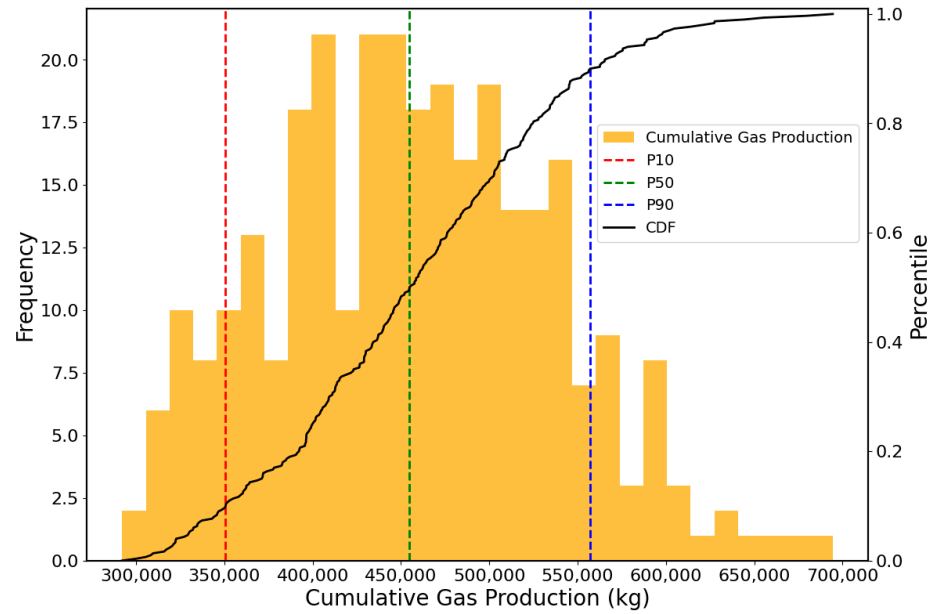
3.3. Uncertainty Analysis

An uncertainty analysis was conducted on 12 key variables identified via sensitivity analysis, employing the LHS technique for an effective Monte Carlo simulation. This analysis involved sampling values for each variable from their respective distribution functions and integrating them to assess the gas and water production potential across different gas hydrate reservoir models. The variables were assumed to follow a uniform distribution, as presented in Table 2. Using LHS, 300 distinct reservoir models were generated to ensure an equitable selection of variable values from their distributions. This methodological approach facilitates thorough uncertainty analysis via an efficient Monte Carlo simulation.

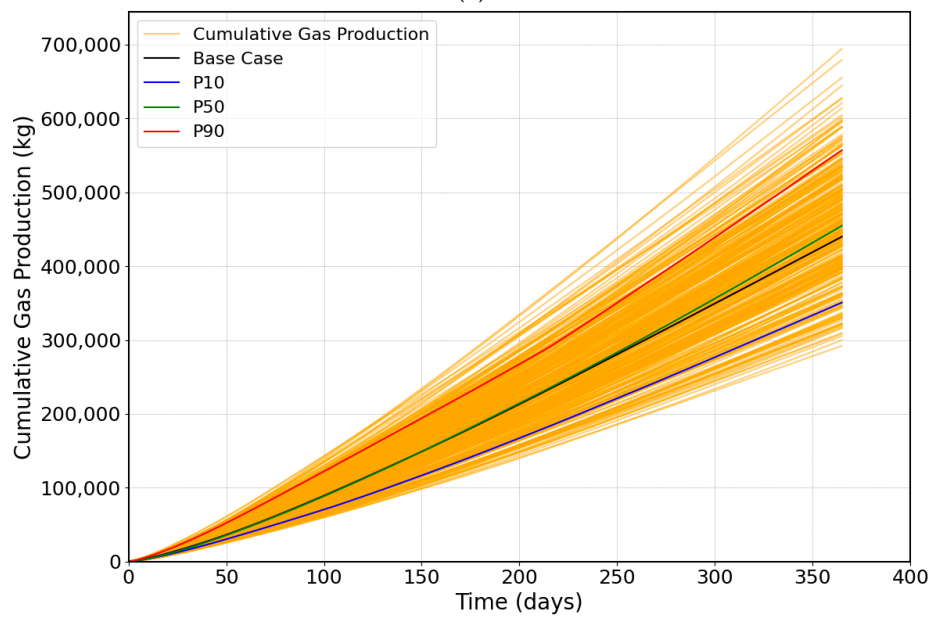
Figure 8 shows an analysis of the cumulative gas production using the TOUGH + HYDRATE simulator, implementing a depressurization strategy at a BHP of 9 MPa. Figure 8a shows a histogram, detailing the cumulative gas production after 1 year, whereas Figure 8b shows the cumulative gas production throughout this period. The black histogram represents the cumulative distribution function. In a study of 300 scenarios, gas production exhibited a general upward trend over the decade with amounts varying from 292 t to 694 t.

Statistical percentiles such as P10, P50, and P90 were employed as critical indicators in the assessment of uncertainty. These measures are essential in both risk management and resource estimation, enabling the determination of production potential and the extent of uncertainty. The P10 percentile indicates the bottom 10% of the dataset, generally offering a conservative projection and is regarded as a proven value with a 90% probability of realization. The P50 value is the median, signifying the probable outcome, whereas P90 represents the possible outcome, indicating an achievable level of production with a 10% likelihood. As shown in Figure 8a, P10 is depicted in blue, P50 in green, and P90 in red. Figure 8b shows the cumulative gas production over time, where the black line denotes the base case results. The findings related to these percentiles are presented in Table 4. The median or P50 value for the cumulative gas production was approximately 455 t.

surpassing the base case figure of 440 t. Figure 9 displays the uncertainty analysis for cumulative water production, with the total water production evaluated ranging between 20,926 and 55,148 t, and the median P50 value was calculated at 32,768 t. Analyzing the results from Table 4, it becomes evident that with property variations within $\pm 20\%$ of the base model values, gas recovery can range from a minimum of 350 t to a maximum of 557 t. Regarding water production, the P90 value is projected at 43,211 t, equating to approximately 118 t/day. Accordingly, facilities for pilot production should be designed to accommodate at least 150 t of daily water production, incorporating a safety margin. Given the substantial volumes of water expected, additional research into effective management techniques for this production is warranted.



(a)

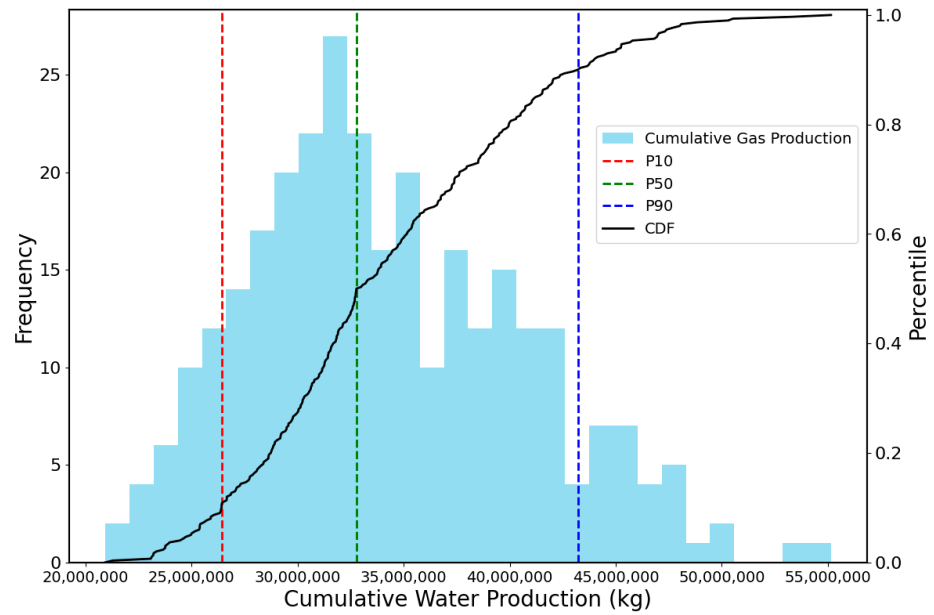


(b)

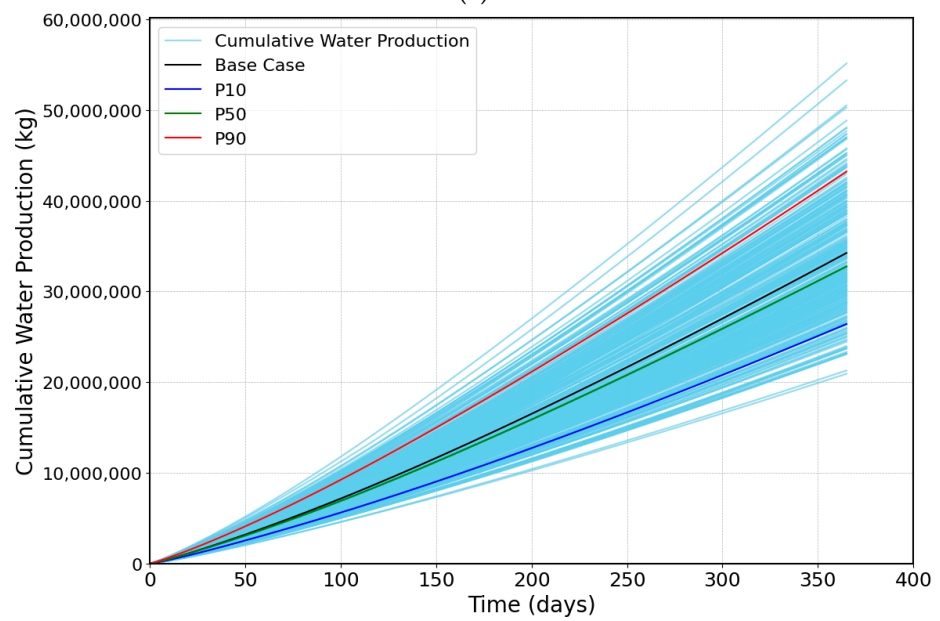
Figure 8. Results of uncertainty analysis conducted on 300 cases of cumulative gas production. (a) Histogram, alongside the percentiles for cumulative gas production after 1 year and (b) cumulative gas production.

Table 4. P10, P50, and P90 of cumulative gas and water production from uncertainty analysis.

Case	Cumulative Gas Production, kg	Cumulative Water Production, kg
P10	350,720	26,411,974
P50	454,787	32,768,290
P90	557,041	43,211,756
Base Case	439,932	34,240,600



(a)



(b)

Figure 9. Results of uncertainty analysis conducted on 300 cases of cumulative water production. (a) histogram, alongside the percentiles for cumulative water production after 1 year and (b) cumulative water production.

A linear correlation analysis was performed on the variables related to the cumulative production of gas and water, as well as their associated uncertainties. This analysis revealed

that the relative permeability of the sand layers exerted the most profound influence on cumulative gas production. Furthermore, the permeability of the sand layers was a critical determinant that affected both the effective permeability within the depressurization zone and the propagation of the hydrate dissociation front. Thermal conductivity significantly impacted cumulative gas production by influencing the thermal variations in the formation, triggered by hydrate dissociation. Although the effect of effective permeability was crucial in the context of cumulative water production, the permeability reduction factor exerted a greater impact than relative permeability. These results underscore the importance of effective permeability and related factors in determining the production efficiency and estimating resources in gas hydrate reservoirs.

In this study, the simulation model was refined to accurately represent the complex reservoir characteristics of UBGH2-6, incorporating statistical analysis methods to comprehensively evaluate production uncertainties. A comprehensive methodology for analyzing gas hydrate reservoirs was developed in this study, which encompasses reservoir modeling, sensitivity analysis, and uncertainty analysis. The research employs an innovative approach by integrating LHS within Monte Carlo simulations, effectively assessing variability and uncertainty across diverse reservoir scenarios for gas hydrate production. The modeling rigor is proven by the detailed evaluation of production outcomes under median and extreme conditions, as indicated by the statistical percentiles P10, P50, and P90. These metrics offer a broad spectrum of potential outcomes, thereby enhancing the decision-making process for field applications. Utilizing these statistical measures to quantify uncertainties significantly aids in understanding the dynamics of gas hydrate dissociation and fluid production, providing crucial insights for optimizing production strategies.

Hydrate dissociation and fluid production are governed by several interconnected physical processes—fluid flow through porous media, heat transfer, phase changes, and kinetic chemical reactions of hydrate dissociation and formation [36,37]. This study utilizes an equilibrium model for field-scale simulations, contrasting with the kinetic models typically employed in laboratory-scale investigations. Additionally, although hydrate distributions in actual field conditions are likely heterogeneous [37,38], the lack of data to quantify this heterogeneity necessitates the assumption that hydrate distributions within individual GHSs are homogeneous, which presents a limitation of this study. Also, the study did not incorporate a detailed correlation analysis of the key variables that influence production behavior. Such intricate analyses are crucial for understanding the interdependencies among variables such as permeability, hydrate saturation, and thermal properties, as well as their collective impact on system performance under diverse operational conditions.

Future research will focus on analyzing hydrate dissociation and gas production behavior under controllable operational scenarios, including depressurization, combined depressurization and thermal injection patterns, and other advanced recovery techniques. By broadening the scope of uncertainty analysis, this study establishes a new standard for predictive accuracy in the field, significantly contributing to the progressive development of gas hydrate technologies.

4. Conclusions

In this study, a simulation model was developed for the UBGH2-6 gas hydrate reservoir in the Ulleung Basin, East Sea, Korea. Through sensitivity analysis, the factors influencing gas and water production were investigated along with their underlying causes. In addition, an LHS-based Monte Carlo simulation was employed to conduct a comprehensive uncertainty analysis, thereby delineating the production characteristics of UBGH2-6. The conclusions drawn from this study are as follows:

- (1) A reservoir simulation model for UBGH2-6 was constructed, featuring 14 thin hydrate-bearing sand layers, with hydrate saturations between 38.8% and 86.2%. Employing a depressurization strategy at 9 MPa to stimulate hydrate production, the model revealed the production of approximately 440 t of gas and 34,240 t of water. This

facilitated an in-depth examination of both the expansion of the depressurization zone and the progression of the hydrate dissociation front.

- (2) The analysis of the production contributions from each layer indicated that sand layer thickness and hydrate saturation levels significantly affected hydrate dissociation. Rapid hydrate dissociation was observed immediately after depressurization commenced in the sand layer, where the hydrate saturation was below 70% and the layer thickness did not exceed 0.2 m. For layers with a thickness exceeding 0.3 m, a suitable period of depressurization was necessary. Upon initiation of dissociation in these thicker layers, a substantial volume of hydrates resulted in an increased production contribution.
- (3) A sensitivity analysis was conducted on the UBGH2-6 reservoir and fluid flow parameters to evaluate their influence on the cumulative production of gas and water. This analysis quantitatively assessed the impact of changes in 19 parameters on production volumes. Results showed that increased porosity and permeability are directly linked to higher production rates. Furthermore, thermal properties were crucial in influencing hydrate dissociation processes, highlighting their significance in the overall dynamics of gas and water production in the reservoir.
- (4) The uncertainty analysis focused on 12 crucial variables identified through a detailed sensitivity analysis and was executed using LHS to enhance the efficiency of the Monte Carlo simulation process. This methodology facilitated the evaluation of 300 distinct reservoir models, enabling a comprehensive assessment of gas and water production potential across a variety of gas hydrate reservoirs for a year. The analysis employed statistical percentiles (P10, P50, and P90) to quantify the degree of uncertainty; the findings revealed a median gas production (P50) of approximately 455 t. This approach underscores the significant impact of key variables on the production potential of gas hydrate reservoirs and provides valuable insights for future exploration and exploitation strategies.

This study identifies critical factors affecting gas hydrate production and offers valuable insights for future exploration and exploitation strategies, making a significant contribution to the field of gas hydrate research.

Author Contributions: Conceptualization, Y.K.; methodology, Y.K. and W.L.; software, Y.K. and W.L.; validation, Y.K. and W.L.; formal analysis, Y.K. and W.L.; investigation, Y.K. and W.L.; writing—original draft preparation, Y.K. and W.L.; writing—review and editing, Y.K. and W.L.; visualization, Y.K.; supervision, W.L. All authors have read and agreed to the published version of the manuscript.

Funding: This research was supported by the Gas Hydrate R&D Organization (GHDO) and the Korea Institute of Geoscience and Mineral Resources (KIGAM) [GP2021-011].

Institutional Review Board Statement: Not applicable.

Informed Consent Statement: Not applicable.

Data Availability Statement: Data are contained within the article.

Conflicts of Interest: The authors declare no conflicts of interest.

References

1. Zheng, R.C.; She, H.B.Y.; Ponnivalavan, B.; Praveen, L.; Xiao-Sen, L. Review of natural gas hydrates as an energy resource: Prospects and challenges. *Appl. Energy* **2016**, *162*, 1633–1652. [[CrossRef](#)]
2. Hou, J.; Zhao, E.; Ji, Y. Numerical simulation of gas production from Class III hydrate reservoirs using low-frequency electric heating-assisted depressurization with horizontal wells. *Fuel* **2024**, *357*, 129906. [[CrossRef](#)]
3. Lei, J.; Wang, Y.; Guo, W. Fines migration characteristics of illite in clayey silt sediments induced by pore water under the depressurization of natural gas hydrate. *Fuel* **2024**, *365*, 131236. [[CrossRef](#)]
4. Gao, F.; Zhang, Y.; Chen, C.; Li, X.; Chen, Z. Numerical Simulation of Hydrate Dissociation Behaviors in Hydrate Reservoir with Different Properties during Horizontal Well Drilling. *J. Mar. Sci. Eng.* **2024**, *12*, 554. [[CrossRef](#)]
5. Yin, Z.; Moridis, G.; Tan, H.K.; Linga, P. Numerical analysis of experimental studies of methane hydrate formation in a sandy porous medium. *Appl. Energy* **2018**, *220*, 681–704. [[CrossRef](#)]

6. Sloan, D. Gas hydrates: Review of physical/chemical properties. *Energy Fuels* **1998**, *12*, 191–196. [[CrossRef](#)]
7. Ndlovu, P.; Babae, S.; Naidoo, P. Review on CH₄-CO₂ replacement for CO₂ sequestration and CH₄/CO₂ hydrate formation in porous media. *Fuel* **2022**, *320*, 123795. [[CrossRef](#)]
8. Giavarini, C.; Hester, K. Methods to predict hydrate formation conditions and formation rate. In *Gas Hydrates*; Springer: London, UK, 2011; pp. 49–57.
9. Chen, Q.; Wu, N.; Liu, C.; Zou, C.; Liu, Y.; Sun, J.; Li, Y.; Hu, G. Research progress on global marine gas hydrate resistivity logging and electrical property experiments. *J. Mar. Sci. Eng.* **2022**, *10*, 645. [[CrossRef](#)]
10. Zyrianova, M.; Collett, T.; Boswell, R. Characterization of the Structural–Stratigraphic and Reservoir Controls on the Occurrence of Gas Hydrates in the Eileen Gas Hydrate Trend, Alaska North Slope. *J. Mar. Sci. Eng.* **2024**, *12*, 472. [[CrossRef](#)]
11. Wan, T.; Li, Z.; Wen, M.; Chen, Z.; Tian, L.; Li, Q.; Qu, J.; Wang, J. Numerical Simulation of Production Behavior with Different Complex Structure Well Types in Class 1-Type Hydrate Reservoir. *J. Mar. Sci. Eng.* **2024**, *12*, 508. [[CrossRef](#)]
12. Huh, D.G.; Lee, J.Y. Overview of gas hydrate R&D. *J. Korean Soc. Miner. Energy Resour. Eng.* **2017**, *54*, 201–214.
13. Korea Institute of Geoscience and Mineral Resources (KIGAM). Gas Hydrate Exploration and Production Study. In *KIGAM Report 19-1143*; KIGAM: Daejeon, Republic of Korea, 2019.
14. Moridis, G.J.; Kim, J.; Reagan, M.T.; Kim, S.J. System response during short- and long-term gas production from a gas hydrate deposit at the site of a planned field test in the Ulleung Basin of the Korean East Sea. In Proceedings of the Offshore Technology Conference, Houston, TX, USA, 4–7 May 2014.
15. Moridis, G.J.; Reagan, M.T.; Queiruga, A.F.; Kim, S.J. System response to gas production from a heterogeneous hydrate accumulation at the UBGH2-6 site of the Ulleung basin in the Korean East Sea. *J. Pet. Sci. Eng.* **2019**, *178*, 655–665. [[CrossRef](#)]
16. Moon, S.Y.; Shin, H.J.; Lim, J.S. Field-scale simulation of gas hydrate dissociation behavior in multilayered sediments under different depressurization conditions. *J. Pet. Sci. Eng.* **2023**, *220*, 111221. [[CrossRef](#)]
17. Lee, T.; Lee, J.Y.; Ahn, T.; Son, H.A. Numerical simulation of gas hydrate production using the cyclic depressurization method in the Ulleung Basin of the Korea East Sea. *Appl. Sci.* **2021**, *11*, 9748. [[CrossRef](#)]
18. Nakajima, C.; Ouchi, H.; Tamaki, M.; Akamine, K.; Sato, M.; Ohtsuki, S.; Naiki, M. Sensitivity and uncertainty analysis for natural gas hydrate production tests in Alaska. *Energy Fuels* **2022**, *36*, 7434–7455. [[CrossRef](#)]
19. Gaddipati, M. Reservoirs modeling of gas hydrate deposits in North Slope of Alaska and Gulf of Mexico. Ph.D. Thesis, West Virginia University, Morgantown, WV, USA, 2014.
20. Yin, Z.; Moridis, G.; Chong, Z.R.; Tan, H.K.; Linga, P. Numerical analysis of experimental studies of methane hydrate dissociation induced by depressurization in a sandy porous medium. *Appl. Energy* **2018**, *230*, 444–459. [[CrossRef](#)]
21. Moridis, G.; Kowalsky, M.; Pruess, K. Depressurization-induced gas production from Class-1 hydrate deposits. In Proceedings of the SPE Annual Technical Conference and Exhibition, Dallas, TX, USA, 9–12 October 2005. [[CrossRef](#)]
22. Moridis, G.; Reagan, M. Strategies for gas production from oceanic Class 3 hydrate accumulations. In Proceedings of the Offshore Technology Conference, Houston, TX, USA, 30 April–3 May 2007. [[CrossRef](#)]
23. Moridis, G.; Reagan, M. Estimating the upper limit of gas production from Class 2 hydrate accumulations in the permafrost: 1. Concepts, system description, and the production base case. *J. Pet. Sci. Eng.* **2011**, *76*, 194–204. [[CrossRef](#)]
24. Moridis, G.; Reagan, M. Estimating the upper limit of gas production from Class 2 hydrate accumulations in the permafrost: 2. Alternative well designs and sensitivity analysis. *J. Pet. Sci. Eng.* **2011**, *76*, 124–137. [[CrossRef](#)]
25. Reagan, M.; Moridis, G.; Johnson, J.; Pan, L.; Freeman, C.; Pan, L.; Boyle, K.; Keen, N.; Husebo, J. Field-scale simulation of production from oceanic gas hydrate deposits. *Transp. Porous Media* **2015**, *108*, 151–169. [[CrossRef](#)]
26. Zheng, R.; Li, S.; Li, X. Sensitivity analysis of hydrate dissociation front conditioned to depressurization and wellbore heating. *Mar. Pet. Geol.* **2018**, *91*, 631–638. [[CrossRef](#)]
27. Tomasini, J.; Stephen, K. Assessment of the potential for gas production from marine methane hydrate reservoirs by numerical simulation. In Proceedings of the SPE Latin American and Caribbean Petroleum Engineering Conference, Virtual, 27–31 July 2020.
28. Masuda, Y.; Naganawa, S.; Ando, S. Numerical calculation of gas-production performance from reservoirs containing natural gas hydrates. In Proceedings of the Western Regional Meeting, Long Beach, CA, USA, 23–27 June 1997.
29. Xu, J.; Bu, Z.; Li, H.; Wang, X.; Liu, S. Permeability Models of Hydrate-Bearing Sediments: A Comprehensive Review with Focus on Normalized Permeability. *Energies* **2022**, *15*, 4524. [[CrossRef](#)]
30. Kim, A.; Kim, H.; Cho, G.; Lee, J. Estimation of model parameters and properties for numerical simulation on geomechanical stability of gas hydrate production in the Ulleung Basin, East Sea, Korea. *Quat. Int.* **2017**, *459*, 55–68. [[CrossRef](#)]
31. Moridis, G.; Collett, T. Strategies for gas production from hydrate accumulation under various geologic conditions. In Proceedings of the TOUGH Symposium, Berkeley, CA, USA, 12–14 May 2003.
32. Lee, J.; Ryu, B.; Yun, T.; Lee, J.; Cho, G. Review on the gas hydrate development and production as a new energy resource. *KSCE J. Civil Eng.* **2011**, *15*, 689–696.
33. Kim, A.R.; Kim, J.Y.; Cho, G.C.; Lee, J.Y. Methane production from marine gas hydrate deposits in Korea: Thermal-hydraulic-mechanical simulation on production wellbore stability. *J. Geophys. Res. Solid Earth* **2018**, *123*, 9555–9569.
34. McKay, M.D.; Beckman, R.J.; Conover, W.J. A comparison of three methods for selecting values of input variables in the analysis of output from a computer code. *Technometrics* **1979**, *21*, 239–245. [[CrossRef](#)]
35. Zheng, R.; Li, S.; Cui, G. Determining the controlling mechanisms of hydrate dissociation front using optimized characteristic time. *Fuel* **2021**, *298*, 120805. [[CrossRef](#)]

36. Li, X.; Xu, C.; Zhang, Y.; Ruan, X.; Li, G.; Wang, Y. Investigation into gas production from natural gas hydrate: A review. *Appl. Energy* **2016**, *172*, 286–322. [[CrossRef](#)]
37. Yin, Z.; Chong, Z.; Tan, H.; Linga, P. Review of gas hydrate dissociation kinetic models for energy recovery. *J. Natural Gas Sci. Eng.* **2016**, *35*, 1362–1387. [[CrossRef](#)]
38. Yin, Z.; Moridis, G.; Linga, P. On the importance of phase saturation heterogeneity in the analysis of laboratory studies of hydrate dissociation. *Appl. Energy* **2019**, *255*, 113861. [[CrossRef](#)]

Disclaimer/Publisher's Note: The statements, opinions and data contained in all publications are solely those of the individual author(s) and contributor(s) and not of MDPI and/or the editor(s). MDPI and/or the editor(s) disclaim responsibility for any injury to people or property resulting from any ideas, methods, instructions or products referred to in the content.